How a solute-pump/solvent-probe spectroscopy can reveal structural dynamics: Polarizability response spectra as a two-dimensional solvation spectroscopy

ARTICLE *in* THE JOURNAL OF CHEMICAL PHYSICS · JULY 2013

Impact Factor: 2.95 · DOI: 10.1063/1.4816373 · Source: PubMed

2 AUTHORS:

Xiang Sun
University of Michigan
5 PUBLICATIONS **13** CITATIONS
SEE PROFILE

Richard M. Stratt
Brown University
122 PUBLICATIONS **4,198** CITATIONS
SEE PROFILE

How a solute-pump/solvent-probe spectroscopy can reveal structural dynamics: Polarizability response spectra as a two-dimensional solvation spectroscopy

Xiang Sun and Richard M. Stratt

Citation: J. Chem. Phys. **139**, 044506 (2013); doi: 10.1063/1.4816373
View online: http://dx.doi.org/10.1063/1.4816373
View Table of Contents: http://jcp.aip.org/resource/1/JCPSA6/v139/i4
Published by the AIP Publishing LLC.

How a solute-pump/solvent-probe spectroscopy can reveal structural dynamics: Polarizability response spectra as a two-dimensional solvation spectroscopy

Xiang Sun and Richard M. Stratt
Department of Chemistry, Brown University, Providence, Rhode Island 02912, USA

(Received 31 May 2013; accepted 9 July 2013; published online 29 July 2013)

The workhorse spectroscopy for studying liquid-state solvation dynamics, time-dependent fluorescence, provides a powerful, but strictly limited, perspective on the solvation process. It forces the evolution of the solute-solvent interaction energy to act as a proxy for what may be fairly involved changes in solvent structure. We suggest that an alternative, a recently demonstrated solute-pump/solvent-probe experiment, can serve as a kind of two-dimensional solvation spectroscopy capable of separating out the structural and energetic aspects of solvation. We begin by showing that one can carry out practical, molecular-level, calculations of these spectra by means of a hybrid theory combining instantaneous-normal-mode ideas with molecular dynamics. Applying the resulting formalism to a model system displaying preferential solvation reveals that the solvent composition changes near the solute do indeed display slow dynamics similar to, but measurably different from, that of the solute-solvent interaction – and that this two-dimensional spectroscopy can effectively single out those local structural changes. © *2013 AIP Publishing LLC*. [http://dx.doi.org/10.1063/1.4816373]

I. INTRODUCTION

By far the most common experimental route for looking at the dynamics of solvation takes advantage of the time-dependent fluorescence of aptly chosen dye molecules.[1,2] The relaxation of a solvent around a newly excited electronic state of the dye solute can substantially lower the solute-solvent potential energy – leading to a time evolution that can be tracked by watching the corresponding decreases in the dye's fluorescence frequency. This several-decade-old idea has now been used to measure solvation dynamics in systems ranging from simple liquids to nucleic acids[3,4] and micelles.[5,6] Photon-echo based methods, such as 3-pulse-photon-echo peak-shift spectra,[7–9] offer an alternative experimental entry into the problem, but these methods continue to rely on variations in the solute's optical gap as the sole indicator of the solvent's dynamics, meaning that they too are monitoring the evolving difference between the excited-state-solute and ground-state-solute potential energies.[2]

But how revealing is the evolution of this single quantity of the full dynamics of solvent rearrangement around a solute? What one would really like to see is the time course of whatever changes there are in the solvent *structure*, which may, or may not, take place on the same time scale as the shifts in solute-solvent potential energy. Suppose, for example, that solute-solvent interactions were dominated by solvent molecules in the first solvation shell, but solvent molecules in the outer shells needed to continue their own repositioning even after the first shell solute-solvent distances were established. Any solute electronic-energy-gap spectroscopy would then be blind to the fact that the full structural relaxation is *slower* than the potential-energy relaxation for such a system. Conversely, if the first solvation shell were again the primary determinant of the solute-solvent potential energy, but considerable rearrangement in the outer-shells were needed before the first solvation-shell population began to have noticeable changes, the spectroscopy would offer no hints that most of the structural relaxation is *faster* than the potential energy relaxation.

The possibility of directly probing the solvent following an electronic excitation of a solute is what has motivated the development of solute-pump/solvent-probe spectroscopy – a two-dimensional (2D) solvation spectroscopy.[10] These experiments are triggered, as in time-dependent-fluorescence studies, by electronically exciting a solute. The observable, however, is not the solute fluorescence, but a time-delayed 4-wave-mixing (effectively, an intermolecular vibrational) spectrum of the surrounding solvent.[11–21] In the resonant-pump polarizability response spectra (RP-PORS) carried out by the Scherer group, for example (Fig. 1),[15–17] a transient-grating spectrum is taken by crossing two non-resonant optical pulses in the sample a time T after the initial resonant solute excitation, and then watching the light scattering from another non-resonant optical pulse a time t after that. The Fourier transform of the response with respect to t yields a Raman spectrum of the solvent, and the evolution of that spectrum with the solvation-progress-time T is what, in principle, could tell us about the solvent's structural evolution.

The initial experimental and theoretical forays into this spectroscopy did not go after this full two-dimensional response.[10,16] They looked only at large T limit, in effect measuring just the difference between the 4-wave-mixing solution spectra with an electronically excited solute and that with a ground-state solute. Nonetheless, the finding that difference could be both observed and understood in molecular

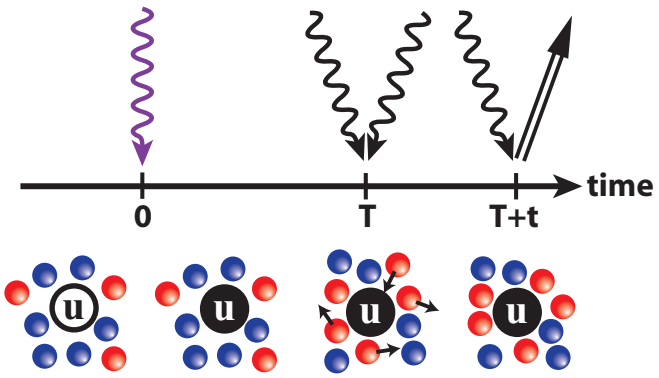

FIG. 1. The sequence of events in solute-pump/solvent-probe spectra. The initial event is an excitation of a solute (u) from its electronic ground electronic state (open black circle) to an excited electronic state (filled black circle) at time 0, with the resulting shift in solute-solvent interactions leading to changes in the structure of the surrounding solvent (colored circles). The experiment monitors the progress of these structural changes by waiting a time T, hitting the sample with a pair of non-resonant visible pulses, waiting for some shorter time t, and then scattering off the sample with a third non-resonant pulse. The time-duration t dynamics reflects the intermolecular vibrations of the liquid (black arrows), so choosing different T values looks at differences in those vibrations as the solvent structure evolves.

terms was promising. Experimental measurements of this difference seemed to be sensitive to the specifics of the solvent, with chemically distinct aprotic dipolar solvents, exhibiting responses of different signs.[16] The same kind of sign changes also showed up in our own theoretical calculations with nonpolar solvent mixtures when we simply adjusted the mole fractions of the solvent components.[10]

Experimental results published since then have made it clear that a complete two-dimensional response is obtainable.[17] The first 2D results for the classic time-dependent-fluorescence system of a coumarin dye dissolved in acetontrile revealed some intriguing fine details about its first 2 ps of solvation. However, since this particular solvent does not seem to undergo any significant large-scale structural rearrangements as it solvates, one might suspect that it is probably not the best candidate for determining whether this kind of spectroscopy can really help us see structural changes.

What we do in this paper is to take the next step. We show, first, that one can calculate the full two-dimensional spectra theoretically from a molecular dynamics simulation, and second, that when the calculated spectra are studied for a system that does undergo major structural rearrangements (in our case, an atomic liquid mixture exhibiting preferential solvation),[10,22,23] the resulting spectra unmistakably do track some of the explicitly structural correlation functions computed from the simulation – correlation functions whose dynamics are measurably different from what would have been seen in time-dependent fluorescence.

The theory we present here builds on our earlier classical-statistical-mechanics analysis of solute-pump/solvent-probe spectra.[10] In that earlier work, we derived a linear-response prediction for the spectroscopy, demonstrating that the spectra are not given by a correlation function of liquid properties at the three times relevant to the 2D experiment (0, T, and $T + t$), but instead reveal the correlation between the triggering solute/solvent potential energy change at time 0 and the Poisson bracket[24] of the solution's many-body polarizability at times T and $T + t$. Evaluating such Poisson brackets can pose a formidable numerical challenge, but we show here how a hybrid calculation judiciously combining molecular-dynamics-based and instantaneous-normal-mode ingredients allows us to evaluate the requisite response functions.

The remainder of this paper is organized as follows: Section II presents our hybrid theory for the two-dimensional response function and shows why the theory offers an apt way of computing two-dimensional spectra. Section III discusses some of the calculational details necessary to implement the theory for our preferential solvation model, and Sec. IV describes our numerical results. We conclude in Sec. V with some general remarks.

II. EVALUATION OF THE SOLUTE-PUMP/SOLVENT-PROBE RESPONSE FUNCTION

A. Linear response theory

Since RP-PORS experiments are designed to compare a 4-wave-mixing signal with and without a resonant pump (solute electronic excitation),[16,17] our main interest is in the difference between the on and off response functions R. Within the classical linear response theory we derived in our previous work,[10] the difference prediction for an experiment of the sort shown in Fig. 1 (with an anisotropic 4-wave mixing probe) is given by

$$\Delta R\left(T+t,T,0\right)=\frac{\left\langle e^{\beta\delta\Delta V(0)}\left\{\Pi_{xz}\left(T\right),\Pi_{xz}\left(T+t\right)\right\}\right\rangle_{e}}{\left\langle e^{\beta\delta\Delta V(0)}\right\rangle_{e}}-\left\langle\left\{\Pi_{xz}\left(T\right),\Pi_{xz}\left(T+t\right)\right\}\right\rangle_{g}. \quad (2.1)$$

Here, $\beta = (k_B T)^{-1}$, the Π_{xz} are the xz components of the many-body polarizability of the system evaluated at the times shown, and the $\Delta V = V_e - V_g$ is the excited-state (e)-solute/ground-state (g)-solute difference in solute-solvent potential energies, evaluated at time 0. Consistent with that notation, the angular brackets with subscripts e and g represent equilibrium averages governed by the solvent-plus-excited-state-solute potential surface, and by the analogous ground-state surface, respectively. The δ refers to fluctuations about the equilibrium average in the relevant state, so in these formulas $\delta\Delta V = \Delta V - \langle\Delta V\rangle_e$. We use the $\{A, B\}$ notation to indicate a Poisson bracket.

It is worth noting that this expression gives the "linear" response in just the limited sense that it captures the part of the spectroscopic response linear in the applied electric fields that couple with the polarizabilities. This same level of treatment for ordinary Raman or optical Kerr spectra yields a response function that can be written in terms of the polarizability autocorrelation function $\langle\Pi(0)\Pi(t)\rangle$ by using standard classical correlation-function identities[24]

$$R\left(t_2,t_1\right)=\left\langle\left\{\Pi_{xz}\left(t_1\right),\Pi_{xz}\left(t_2\right)\right\}\right\rangle=-\beta\left[\frac{d}{dt}\left\langle\Pi_{xz}\left(0\right)\Pi_{xz}\left(t\right)\right\rangle\right]_{t=t_2-t_1}. \quad (2.2)$$

This formula is what is behind the textbook result that the frequency-domain Raman spectra are Fourier transforms of polarizability autocorrelation functions.[25] Our theory does not, however, linearize with respect to the optical gap ΔV, as is usually done in linear-response treatments of time-dependent fluorescence.[26] This latter form of linear response is what is used to identify $S(t)$, the normalized relaxation of the non-equilibrium-average fluorescence frequency ($\overline{\nu(t)}$), with $C_{\Delta V}(t)$, the normalized e-g potential-energy-difference autocorrelation function,

$$\begin{aligned} S(t) &= \left(\overline{\nu(t)} - \overline{\nu(\infty)}\right) / \left(\overline{\nu(0)} - \overline{\nu(\infty)}\right) \\ C_{\Delta V}(t) &= \langle \delta\Delta V(0)\, \delta\Delta V(t)\rangle_e / \langle (\delta\Delta V)^2\rangle_e. \end{aligned} \tag{2.3}$$

This extra approximation is normally (although not always) remarkably accurate,[1,27] though it turns out not to be necessary for our calculations here. Nonetheless, this additional linearization does allow us to obtain a nice physical interpretation. If we take this extra step, Eq. (2.1) becomes

$$\begin{aligned} \Delta R(T+t, T, 0) = -\beta \frac{d}{dt} [&\langle \Pi_{xz}(0)\, \Pi_{xz}(t)\rangle_e \\ &- \langle \Pi_{xz}(0)\, \Pi_{xz}(t)\rangle_g] \\ &-\beta \langle \delta\Delta V(0) \{\Pi_{xz}(T), \Pi_{xz}(T+t)\}\rangle_e . \end{aligned} \tag{2.4}$$

The first two terms, which depend only on the time interval t, are simply the difference between the equilibrated OKE spectra for the excited- and ground-state solutions: the $T \to \infty$ limit of our experiment. The last term, however, is the correlation between the time-zero solute-optical-gap fluctuation and the results of the subsequent light scattering. This quantity is a genuine 3-time average incorporating all of the two-dimensional information in our experiment.

Poisson brackets $\{A(0), B(t)\}$, such as those in this last term, can be thought of a measures of the sensitivity of some function at time t, $B(t)$, to variations in a function at time 0, $A(0)$,

$$\{A(0), B(t)\} = \sum_{k=1}^{3N} \left[\frac{\partial A(0)}{\partial r_k(0)} \frac{\partial B(t)}{\partial p_k(0)} - \frac{\partial A(0)}{\partial p_k(0)} \frac{\partial B(t)}{\partial r_k(0)} \right], \tag{2.5}$$

where the sum is over all the 3N degrees of freedom of our N-particle system, and the $p_k(0)$ and $r_k(0)$ are the momenta and coordinates for the kth degree of freedom at time 0. So what the experiment really looks at is the evolution, as the memory of the solute electronic excitations starts to fade, of the sensitivity of the polarizability to its value at a slightly earlier time – which, in practice, means the evolution of the solvent's intermolecular vibrations as the solvent structure reorganizes.

B. Hybrid instantaneous-normal-mode/molecular dynamics evaluation

Equation (2.1) (or Eq. (2.4)) can, in principle, be evaluated by carrying out nested molecular dynamics calculations. One can start with a long "primary" classical trajectory (of some duration greater than the liquid's structural relaxation times) and sample it at each desired value of the solvation delay time T. The Poisson brackets $\{\Pi(T), \Pi(T+t)\}$, can then be calculated for the specified T values by using a series of "secondary" ($T \to T+t$) trajectories: Since the many-body polarizabilities at a given time depend only on the instantaneous liquid configuration $\mathbf{R} = \{r_k; (k = 1, \ldots, 3N)\}$, Eq. (2.5) implies

$$\begin{aligned} \{\Pi(T), \Pi(T+t)\} &= \{\Pi[\mathbf{R}(T)], \Pi[\mathbf{R}(T+t)]\} \\ &= \sum_{i,k=1}^{3N} \left[\left(\frac{\partial \Pi}{\partial r_i}\right)_T \left(\frac{\partial \Pi}{\partial r_k}\right)_{T+t} \frac{\partial r_k(T+t)}{\partial p_i(T)} \right], \end{aligned} \tag{2.6}$$

meaning that the necessary $\partial r(T+t)/\partial p(T)$ derivatives can be computed by finite difference with respect to the $p(T)$ initial conditions of the secondary ($T \to T+t$) trajectories.[28]

This procedure has, in fact, been successfully applied in multidimensional spectroscopy simulations,[24,29–31] but the practical difficulty it faces is that Poisson brackets are essentially fluctuation quantities, making them intrinsically noisy to simulate, and looking for their correlation with yet another fluctuation makes the numerical situation even worse.[30,32,33] One approach to circumventing these problems has been to avoid linear response altogether by simulating the non-equilibrium response in the presence of explicit applied fields.[34–36] There have also been more recent approaches combining equilibrium and non-equilibrium trajectories.[37–39] Such simulations can be useful in practice, but they sacrifice the conceptual advantages of allowing us to analyze the results in terms of equilibrium average properties of the system. On the analytical side, there have also been attempts to approximate the Poisson brackets in such a way as to end up with ordinary correlation functions. Some of these have made use of generalized-Langevin-equation[40,41] and mode-coupling[42–47] frameworks, but there has also been a novel formulation in which the classical results have been predicted based on approximations to the quantum mechanical analogue.[48–52]

We propose yet another approach here. What turned out to be key for our purposes was the realization that for the kinds of problems of interest in solvation spectroscopy, the time scales T and t are usually going to be widely separated. While T must be long enough to see whatever large-scale reorganization dynamics there is in the liquid, t needs only to be large enough to capture the most-telling intermolecular vibrations. For vibrations with frequencies larger than 50 cm^{-1} or so, that means sub-ps values of t.

But, for any such relatively high-frequency parts of the intermolecular motion, the *instantaneous normal modes* (INMs) of the liquid[53–55] do a reasonably faithful job in representing the dynamics[56,57] – and since that dynamics can be evaluated analytically in terms of the initial conditions, that means that the $\{\Pi(T), \Pi(T+t)\}$ Poisson brackets can be evaluated analytically in terms of molecular dynamics information available from the primary trajectory at each desired time T.[58] The end result is a kind of hybrid calculation combining exact molecular dynamics with INM techniques. The way this works is as follows: In INM dynamics, the propagation

of the system's configuration from any instantaneous liquid configuration $\mathbf{R_0}$ to $\mathbf{R_t}$, its configuration a (short) time t later, is considered to be governed solely by the part of its potential energy V derived by expanding through second order in mass-weighted displacement $\delta\mathbf{Z_t} = \boldsymbol{M}^{1/2} \cdot (\mathbf{R_t} - \mathbf{R_0})$ about the instantaneous configuration[54]

$$V(\mathbf{R_t}) = V(\mathbf{R_0}) + \nabla V(\mathbf{R_0}) \cdot (\delta\mathbf{Z_t}) + \frac{1}{2}\delta\mathbf{Z_t} \cdot \nabla\nabla V(\mathbf{R_0}) \cdot \delta\mathbf{Z_t}. \quad (2.7)$$

Here the gradients denote derivatives with respect to mass-weighted coordinates $\mathbf{Z}$.

For a liquid with N atoms, all of mass m, whose positions are described using Cartesian coordinates, for example, the matrix $\boldsymbol{M} = (m)\boldsymbol{1}$, with $\boldsymbol{1}$ the $3N \times 3N$ identity matrix. The matrix of instantaneous eigenvectors $\boldsymbol{U}(R_0)$ of the $3N \times 3N$ matrix $\nabla\nabla V(R_0)$ then determines what, in a sense, is the optimum basis for describing the short-time dynamics – the instantaneous normal modes $q_\alpha(t;\mathbf{R_0})$, $\alpha = (1, \ldots, 3N)$,

$$\begin{aligned}
[\boldsymbol{U}(\mathbf{R_0}) \cdot \nabla\nabla V(\mathbf{R_0}) \cdot \boldsymbol{U}^{tr}(\mathbf{R_0})]_{\alpha\beta} &= \delta_{\alpha\beta}\,\omega_\alpha^2(\mathbf{R_0}), \quad (\alpha, \beta = 1, \ldots, 3\mathrm{N}) \\
q_\alpha(t;\mathbf{R_0}) &= [\boldsymbol{U}(\mathbf{R_0}) \cdot \delta\mathbf{Z_t}]_\alpha, \quad (\alpha = 1, \ldots, 3\mathrm{N}) \\
p_\alpha(t;\mathbf{R_0}) &= [\boldsymbol{U}(\mathbf{R_0}) \cdot \delta\dot{\mathbf{Z}}_\mathbf{t}]_\alpha, \ (\alpha = 1, \ldots, 3\mathrm{N}).
\end{aligned} \quad (2.8)$$

Since the displacements q_α are small at short times, we can evaluate Eq. (2.6) by taking the relevant instantaneous configuration to be $\mathbf{R_T}$, transforming to that INM basis, and keeping only the leading contribution in powers of the $q_\alpha(t;\mathbf{R_T})$,

$$\begin{aligned}
\{\Pi(T), \Pi(T+t)\} &= \sum_{\alpha,\beta=1}^{3N} \left[\Pi_\alpha(T)\,\Pi_\beta(T+t)\,\frac{\partial q_\beta(t;\mathbf{R_T})}{\partial p_\alpha(0;\mathbf{R_T})}\right] \\
&\approx \sum_{\alpha,\beta=1}^{3N} \left[\Pi_\alpha(T)\,\Pi_\beta(T)\,\frac{\partial q_\beta(t;\mathbf{R_T})}{\partial p_\alpha(0;\mathbf{R_T})}\right],
\end{aligned} \quad (2.9)$$

where the quantities

$$\Pi_\alpha(T) \equiv \left.\frac{\partial\Pi}{\partial q_\alpha}\right|_T \equiv \frac{1}{\sqrt{m}}\sum_{i=1}^{3N}\left.\frac{\partial\Pi}{\partial r_i}\right|_T U_{i,\alpha}^{tr}(\mathbf{R_T}) \quad (2.10)$$

represent the instantaneous susceptibilities of the polarizability to displacements along the αth direction. But since the INM modes are mutually orthogonal and the dynamics of each mode α is harmonic with a frequency $\omega_\alpha(\mathbf{R_T})$,

$$\frac{\partial q_\beta(t;\mathbf{R_T})}{\partial p_\alpha(0;\mathbf{R_T})} = \delta_{\alpha\beta}\frac{\sin[\omega_\alpha(\mathbf{R_T})\,t]}{\omega_\alpha(\mathbf{R_T})},$$

the desired Poisson bracket is then simply

$$\{\Pi(T), \Pi(T+t)\} = \sum_{\alpha=1}^{3N}\Pi_\alpha^2(T)\frac{\sin[\omega_\alpha(T)\,t]}{\omega_\alpha(T)}, \quad (2.11)$$

with $\omega_\alpha(T) \equiv \omega_\alpha(\mathbf{R_T})$.[58]

This hybrid INM formulation makes it particularly straightforward to write our overall response function in a physically revealing fashion, with the structural relaxation time T specified in the time domain, but the intermolecular vibration times t expressed in the frequency domain. Since we need the imaginary part of the response,[15,16,59] the desired spectroscopic response function is

$$\Delta R(\omega;T) = \int_0^\infty dt \sin\omega t\,\Delta R(T+t, T, 0), \quad (2.12)$$

which becomes, with the aid of Eqs. (2.1) and (2.11),

$$\begin{aligned}
\Delta R(\omega;T) = \frac{\pi}{2\omega}&\frac{\left\langle e^{\beta\delta\Delta V(0)}\sum_{\alpha=1}^{3N}\Pi_{xz,\alpha}^2(T)\,\delta(\omega-\omega_\alpha(T))\right\rangle_e}{\langle e^{\beta\delta\Delta V(0)}\rangle_e} \\
&-\frac{\pi}{2\omega}\left\langle\sum_{\alpha=1}^{3N}\Pi_{xz,\alpha}^2\delta(\omega-\omega_\alpha)\right\rangle_g.
\end{aligned} \quad (2.13)$$

Equation (2.13) is our principal result. This last term in this equation is simply the ground-state INM density of states weighted by the susceptibilities of the (xz-component of the) many-body polarizability to motion along each INM mode. That is, it is just the INM approximation for the optical Kerr spectrum of the liquid with the solute in its ground state.[57] Since there is no solute excitation to give any significance to time T, this part of the spectrum is independent of T. The first term in Eq. (2.13) is also an INM spectrum, but it not only focuses on the dynamics with an excited-state-solute, it depends explicitly on the time delay T because it measures the correlations between time-zero solute-solvent potential energy fluctuations and time-T polarizability susceptibilities.

How accurate is our INM approximation likely to be?[60] It is certainly surprising that we would even contemplate using an explicitly short-time theory such as INM theory in the middle of a calculation of long-time dynamics. But what makes this approach sensible is the hybrid character of the formalism – which relies on molecular dynamics for any protracted time evolution, and uses INM answers solely for the high frequency features. Our experience with predicting OKE spectroscopy suggests that the segments of our results that largely reflect high-frequency equilibrium OKE spectra should be handled quite well.[57] Consider the preferential

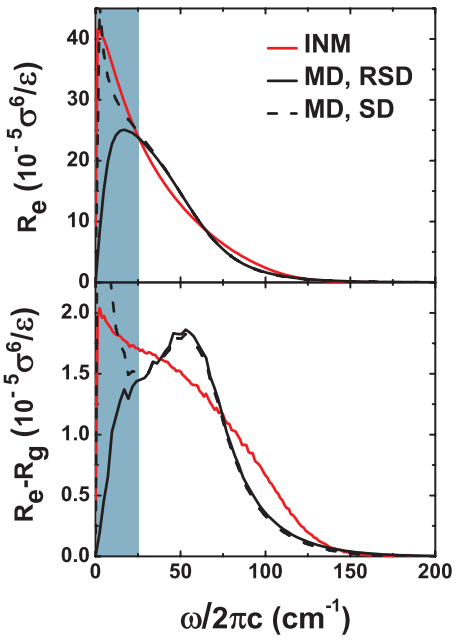

FIG. 2. Comparison of exact-molecular-dynamics (MD) and instantaneous-normal-mode (INM) predictions of optical Kerr spectra for the solute-plus-(10% S)-solvent-mixture system described in Sec. III. The upper panel is the OKE spectrum of the system with an excited-state solute; the lower panel is the difference between the OKE spectra with excited- and ground-state solutes. Note the (more than) order-of-magnitude difference in vertical scales between the two panels. Molecular dynamics results are reported (as described in Ref. 62) both as reduced spectral densities (RSD, solid black lines) and as full spectral densities (SD, dashed black lines). Both MD and INM calculations use a single solute + 255 solvents and first-order treatments of the polarizability. MD results are averaged over 1×10^8 liquid configurations, INM results over 1.6×10^6 configurations and only real INM frequencies are shown. The marked differences between INM and exact results in the low-frequency (shaded) region of the lower panel are a reminder that the INM methods we use here are not suitable for this domain. See Ref. 60 for further discussion of this point.

solvation model system we studied in our previous work.[10] As the top panel of Fig. 2 makes clear, the reduced OKE spectrum of the solution with an excited-state solute nicely matches the exact molecular dynamics results for the model, Eq. (2.2), at least for frequencies above 25 cm^{-1} – although it deviates rather strongly below this frequency.[61,62] The full solute-pump/solvent-probe spectrum reflects fine distinctions between excited- and ground-state dynamics, and is therefore a potentially more challenging test of the dynamical details. Nonetheless the bottom panel of Fig. 2 shows that INM theory also does a respectable (though less quantitative) job of handling the difference between excited-state and ground-state OKE spectra (the $T \to \infty$ limit of the two-dimensional spectra).

It is interesting, as well, to take a step back from the specifics of this solute-pump/solvent-probe spectroscopy and look more generally at how well INM approaches handle the kinds of Poisson brackets that invariably show up in multidimensional spectroscopy.[58] Compared to other approximations proposed in the literature, how well do expressions such as Eq. (2.11) fare? As we detail in the Appendix, Eq. (2.11) is the result of a linearized INM treatment, one in which fluctuations of spectroscopic observables are assumed to be linear in coordinate displacements.[63–66] In the absence of such linearizations, INM formulas will always be correct at short times, accurate at high frequencies, and (not surprisingly) exact for all times whenever the dynamics is truly harmonic. There are going to be other criteria we should measure this formalism against in comparing with literature alternatives (including how much better those methods are at representing *anharmonic* effects),[58] but it appears that the hybrid-INM/MD approach is particularly well suited to situations with the kind of time-scale separations we encounter with solute-pump/solvent-probe spectroscopy. We offer some detailed comparisons in the Appendix.

III. MODELS AND METHODS

A. The preferential solvation model and its dynamics

The system we study here is the same one outlined in a number of earlier papers:[10,22,23] an atomic liquid mixture consisting of a single solute (u) and mixture of strongly (S) and more-weakly (W) solvating solvent atoms. All of the atoms have identical masses m and interact via identical Lennard-Jones potentials whenever the solute is in its ground electronic state (u-g), but when the solute is promoted to its excited electronic state (u-e), the solute-solvent attractions increase, and they do so differentially for the S and W solvents

$$\begin{aligned} u_{ab}(r) &= 4\varepsilon_{ab}[(\sigma_{ab}/r)^{12} - (\sigma_{ab}/r)^6], \\ a, b &= u\text{-}g, u\text{-}e, S, W \\ \sigma_{ab} &= \sigma, \quad \text{(all interactions)} \\ \varepsilon_{ab} &= \varepsilon, \quad \text{(all interactions except those involving } u\text{-}e) \\ \varepsilon_{u\text{-}e,S} &= 3\varepsilon, \quad \varepsilon_{u\text{-}e,W} = 1.5\varepsilon. \end{aligned} \tag{3.1}$$

The solution densities and temperatures are fixed at $\rho\sigma^3 = 0.80$ and $k_BT/\varepsilon = 1.00 \pm 0.03$, respectively, and we define our time scale by choosing standard Ar parameters: $m = 39.948$ amu, $\sigma = 3.405$ Å, $\varepsilon/k_B = 119.8$ K (corresponding to a Lennard-Jones time unit $\tau_{LJ} = 2.16$ ps).

As simple as this system is, it showcases the classic phenomenology of preferential solvation,[67–69] Fig. 3. The solvation-energy correlation functions defined in Eq. (2.3) reflect the expected sub-picosecond relaxation for each of the pure solvents (100% S and 0% S), but mixing the two solvents noticeably slows the relaxation, with our very slowest relaxation occurring for 10% S solvent (the system we focus on for the remainder of the paper). The slowness of the potential energy relaxation in mixed solvents is clearly tied in with the extra structural reorganization needed to form an equilibrated solvent distribution around a newly excited solute.[22,68] In the 10% case, the solute's desire to replace W solvents with S solvents in the first solvation shell results in the average first solvation shell populations having to shift from (1.3 S, 11 W) to (3.0 S, 9.7 W).[10] These changes in first-shell numbers may not seem all that large, but as we saw in our potential-energy-landscape analysis of this problem,[22] the sequence of solvent motions needed to achieve them is rather lengthy. The basic question in this paper, in fact, is whether such specific features of the structural reorganization can show up in a spectroscopic measurement.

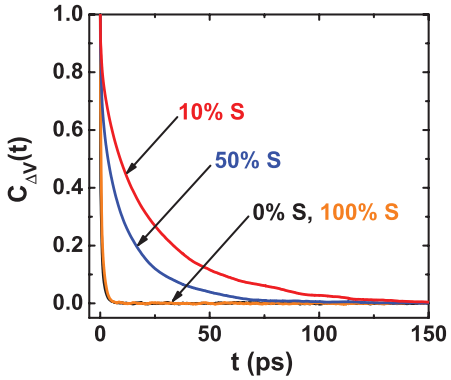

FIG. 3. Solvation dynamics for the preferential solvation model described in the text. The graph plots the normalized solute/solvent potential energy correlation function $C_{\Delta V}$ versus time t for 4 different mixtures of strongly solvating (S) and weakly solvating (W) solvent atoms. On the scale shown, the neat strong solvent (100% S) and neat weak solvent (0% S) cases exhibit virtually identical ultrafast relaxations. The corresponding non-equilibrium response functions for all 4 of these mixtures (not shown) match these curves nearly perfectly on this scale (see Ref. 10, Fig. 3). All of the curves plotted are for single solute + 255 solvent atom systems averaged over 5×10^6 liquid configurations.

Molecular dynamics simulations of the model were carried out by velocity-Verlet integration[70] with a time step $\delta t = 2.5 \times 10^{-3}\ \tau_{\rm LJ} = 5.4$ fs, and averages computed by sampling the resulting liquid configurations every 10 time steps. Equilibrations were performed using standard protocols.[61]

B. Spectroscopic calculations

The expressions for the optical Kerr and 2D-spectra both rely on evaluating the system's many-body polarizability tensor $\mathbf{\Pi}$ at each liquid configuration. To that end, we choose polarizabilities for the solute and the S and W solvents that are the same as in our earlier work[10]

$$\alpha_u = 0.2\sigma^3 = 7.90\,\text{Å}^3, \quad \alpha_S = 0.101\sigma^3 = 3.99\text{Å}^3,$$
$$\alpha_W = 0.0186\sigma^3 = 0.73\text{Å}^3.$$

That choice, consistent with realistic solute chromophores, assigns the solute the largest polarizability in the system,[71] and motivated by such preferential-solvation cosolvents such as dimethyl sulfoxide/water,[72] associates the more strongly solvating solvent with the larger of the two remaining polarizabilities. (Unlike the experimental situation, though, our solute polarizability does not change with electronic state).[71]

The full many-body polarizability is a self-consistent sum of interaction-induced terms, and, indeed, the dynamics of our atomic-mixture system is only revealed by a polarizability spectroscopy because those interaction-induced terms evolve as the interatomic distances evolve. To leading order for an N-atom system,

$$\mathbf{\Pi} = \sum_{j=1}^{N} \boldsymbol{\pi}_j, \quad \boldsymbol{\pi}_j = \boldsymbol{\alpha}_j + \sum_{k\neq j}^{N} \boldsymbol{\alpha}_j \cdot \mathbf{T}_{jk} \cdot \boldsymbol{\alpha}_k, \tag{3.2}$$

where $\boldsymbol{\alpha}_j$ is the polarizability tensor for the jth atom and the $\mathbf{T}_{jk}$ are dipole-dipole interaction tensors (which depend on the interatomic displacements $\mathbf{r}_{jk} = \mathbf{r}_j - \mathbf{r}_k$),[73]

$$\boldsymbol{\alpha}_j = \alpha_j \mathbf{1}, \quad \mathbf{T}_{jk} = \left[(3\hat{r}\hat{r} - \mathbf{1})/r^3\right]_{\mathbf{r}=\mathbf{r}_{jk}}. \tag{3.3}$$

Our previous study showed that the first-order dipole-induced-dipole approximation given in Eq. (3.2) does a reasonable job of capturing the polarizability dynamics of our preferential solvation system (although it cannot be counted in to reproduce the absolute magnitudes of spectroscopic response functions).[10] To reduce the computational burden, we will therefore limit ourselves to this first-order treatment for all of the calculations in this paper.

The quantities needed for evaluating our anisotropic response functions, Eq. (2.13) involves only the xz element of the $\mathbf{\Pi}$ tensors.[59] However, we further reduce the calculational noise by deriving the desired element from the full rotational invariants of the $\mathbf{\Pi}$ tensor,[74] meaning that polarizability derivatives such as those in Eq. (2.13) are evaluated as

$$\left\langle \Pi^2_{xz,\alpha} \right\rangle_{\substack{rotationally \\ averaged}} = \tfrac{1}{10} PP\left(\frac{\partial \mathbf{\Pi}}{\partial q_\alpha}, \frac{\partial \mathbf{\Pi}}{\partial q_\alpha}\right) - \tfrac{1}{30}\left[Tr\left(\frac{\partial \mathbf{\Pi}}{\partial q_\alpha}\right)\right]^2 \tag{3.4}$$

$$PP(\mathbf{A},\mathbf{B}) = \sum_{\mu,\nu=x,y,z} A_{\mu\nu} B_{\mu\nu}, \quad Tr(\mathbf{A}) = \sum_{\mu=x,y,z} A_{\mu\mu}.$$

Instantaneous normal modes are computed by diagonalizing the $\nabla\nabla V$ dynamical matrix (Eq. (2.8)) using the LAPACK software library.[75]

IV. RESULTS

The predictions of Eq. (2.13) for the two-dimensional solvation spectrum of our model are shown in Fig. 4. We know from Fig. 2 that the INM analysis is likely to seriously overestimate the response for frequencies $\omega/(2\pi c) < 25\ \text{cm}^{-1}$, so it is probably best to focus on the results for frequencies higher than 25 cm^{-1}. In that higher frequency range though, we can clearly see the progression of the intermolecular-vibration part of the spectrum from its instantaneous appearance immediately after the solute excitation ($T = 0$) towards the equilibrated excited-state/ground-state difference spectrum (e-g) within 50–100 ps.

Times intervals in this range are broadly consistent with the kinds of time scale expected from the 10% S solvation correlation function, Fig. 3. However, it is worth being a bit more quantitative in specifying the features of the liquid's dynamics the spectroscopy is most sensitive to. We can construct a normalized relaxation profile for the spectrum at any given intermolecular-vibration frequency ω by defining

$$S(T;\omega) = \frac{\Delta R(\omega;T) - \Delta R(\omega;T=\infty)}{\Delta R(\omega;T=0) - \Delta R(\omega;T=\infty)}. \tag{4.1}$$

As we can see in Fig. 5, this $S(T)$ is virtually the same at $\omega/(2\pi c) = 50\ \text{cm}^{-1}$ as it is at 75 cm^{-1}, whereas both profiles

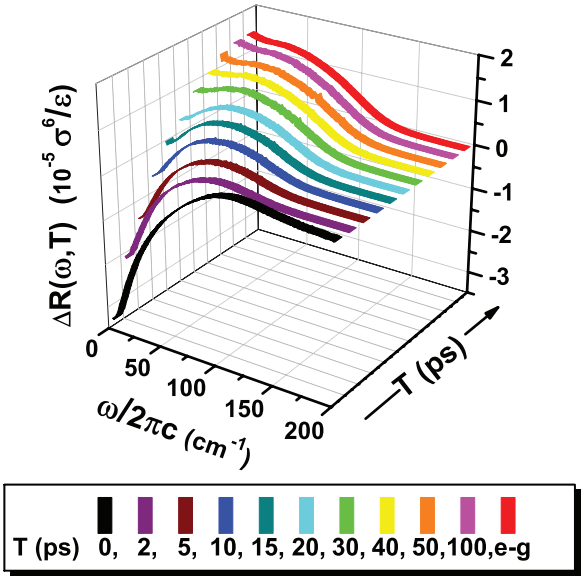

FIG. 4. Two-dimensional solute-pump/solvent-probe spectra for our (10% S) preferential solvation system calculated by hybrid INM/molecular-dynamics methods. The spectra show how the solution's intermolecular vibrational spectrum (reported as a function of ω) evolves with increasing delay time T since excitation of a probe solute. The large T limit (labeled e-g) is the same difference between excited- and ground-state-solute INM optical Kerr spectra reported in Fig. 2. The results shown are for a single solute + 107 solvent atom system averaged over 1.6×10^7 liquid configurations using first-order many-body polarizabilities.

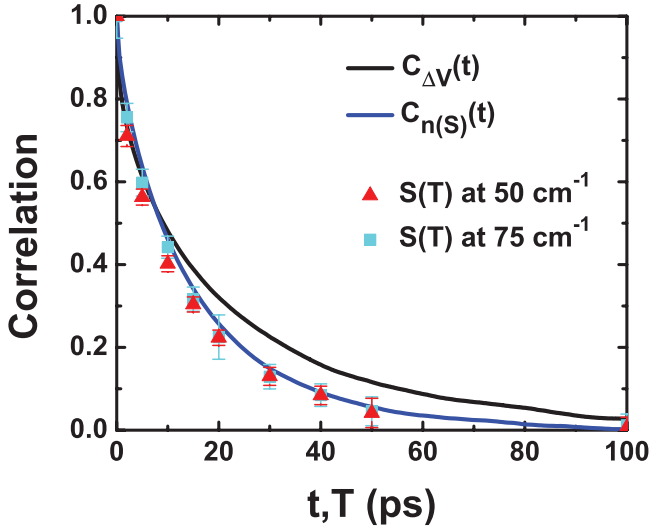

FIG. 5. Comparison of the relaxation dynamics observed by solute-pump/solvent-probe spectra with both structure- and potential-energy-sensitive equilibrium solvation correlation functions for our (10% S) preferential solvation system. Dynamics is extracted from the spectroscopy reported in Fig. 4 by looking at the spectroscopic response functions $\Delta R(\omega, T)$ as a function of solvation time T for fixed intermolecular frequencies ω. Normalized versions of these response function, $S(T)$, are shown here as triangles and squares for $\omega/(2\pi c) = 50$ and 75 cm^{-1}, respectively. The potential energy-sensitive measure (black line) is the standard solvation correlation function (the same $C_{\Delta V}(t)$ function reported in Fig. 3). The structure-sensitive measure (blue line) is the normalized correlation function for the number of strong solvent in the first solvation shell, $C_{n(S)}(t)$. This last correlation function was computed by averaging a 108-atom solution over 9.2×10^5 configurations.

are noticeably faster than the solute-solvent potential energy relaxation tracked by the $C_{\Delta V}(t)$ solvation correlation function of Eq. (2.3).

But what if we were to look at some correlation function that directly measured the structural relaxation? Suppose, for example, we defined n_S to be the number of S solvents in the first solvation shell of the solute and examined how its fluctuations $\delta n_S = n_S - \langle n_S \rangle_e$ relaxed[76]

$$C_{n_S}(t) = \langle \delta n_S(0)\, \delta n_S(t) \rangle_e / \langle (\delta n_S)^2 \rangle_e. \quad (4.2)$$

Figure 5 shows a remarkable agreement between this structural correlation function and the spectroscopic profiles $S(T)$. In fact, even the mixed potential-energy/structure correlation functions (not shown)

$$C_{\Delta V, n_S}(t) = \langle \delta\Delta V(0)\, \delta n_S(t) \rangle_e / \langle (\delta\Delta V)(\delta n_S) \rangle_e \quad (4.3)$$

agree quantitatively with the $S(T)$ profiles. To the limited, but nonetheless measurable, extent that structural and energetic dynamics do differ in this system, the two-dimensional spectroscopy seems to be selectively picking up on the explicitly structural dynamics.

So what makes this spectroscopy such a good structural probe? Our studies of the $T \to \infty$ results in our previous work indicated that solvation shells beyond the first contribute significantly to the overall signal,[10] so it may not obvious why there should be such a close connection with the first shell population dynamics. The answer may lie in precisely how solvation shell populations change. Look, in particular, at how the distribution of strong-solvent/solute/strong-solvent angles θ changes with time T elapsed since the solute excitation, Fig. 6.

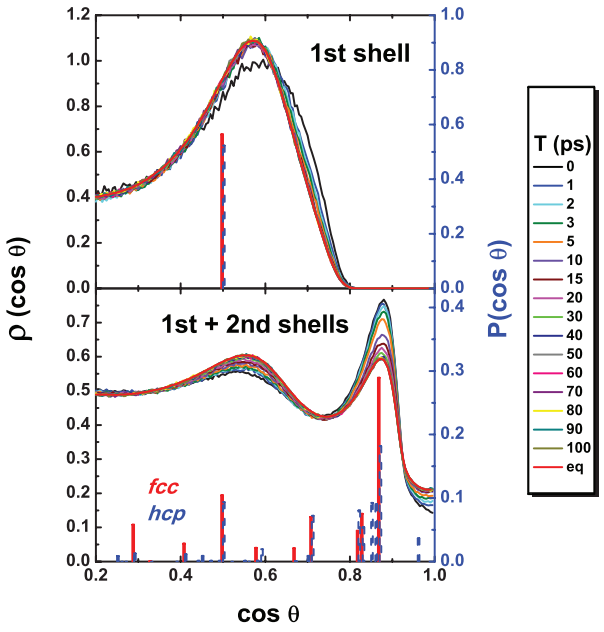

FIG. 6. The evolution of solvent structure around the solute in our 10% S preferential solvation system. The curves show how the probability densities, $\rho(\cos\theta)$ of solvent-solute-solvent angles θ change with the time T elapsed since solute excitation. For comparison, we report what the probability distribution of these angles would be, $P(\cos\theta)$, if a solution with the same density and solvent composition were arranged in a perfect fcc lattice (solid red vertical lines) or in a perfect hcp lattice (dashed blue vertical lines). The upper panel looks only at solvent in the first solvation shell; the lower panel includes solvents in both the first and second solvation shells. $\rho(\cos\theta)$ curves represent non-equilibrium averages of 108-atom solutions over 5×10^5 initial conditions.

If we call R the set of strong solvents we are interested in, define $\hat{r}_{0j}$ and $\hat{r}_{0k}$ to be unit vectors pointing from the solute to solvents j and k, and let $n_{\mathsf{R}}(SS)$ be the number of S-S solvent pairs in the indicated region, then the non-equilibrium-average probability densities of these angles are given by[77–80]

$$\rho\left(\cos\theta\right)_T = \overline{\frac{1}{n_{\mathsf{R}}(SS)} \sum_{(j<k)\in \mathsf{R}} \delta(\cos\theta - \hat{r}_{0j}\left(T\right)\cdot\hat{r}_{0k}\left(T\right))}. \tag{4.4}$$

Figure 6 reveals that the most significant shifts in this distribution occur when it encompasses *both* 1st and 2nd shell solvent atoms. The 1st shell solvent distribution exhibits a small initial sub-picosecond shift, but from that point on remains consistently peaked at angles near 55° ($\cos\theta \approx 0.57$) (while the 2nd shell distribution (not shown) shows no visible evolution at all). The joint 1st and 2nd shell distribution, though, shows a slow decrease in angles near 30° ($\cos\theta \approx 0.87$) and a simultaneous increase in first-shell-like angles.

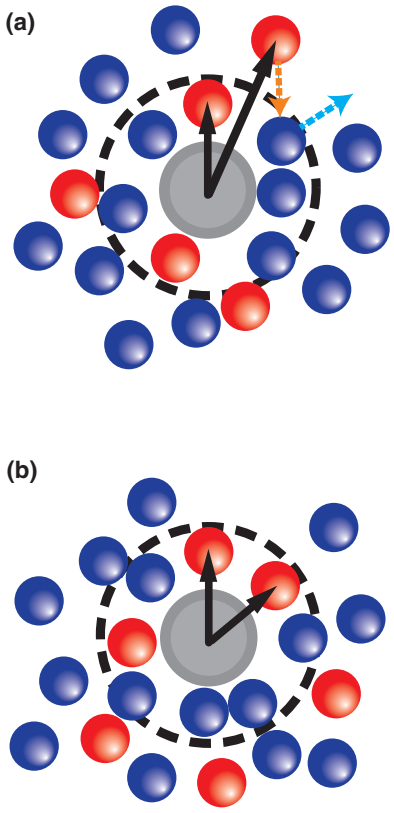

FIG. 7. Schematic picture of how the solvent structure responds to solute excitation in a preferential solvation system. (a) Before the solute (central grey circle) is excited, the first solvation shell (the region inside the dashed circle) contains the ground-state equilibrium fraction of strong (red) and weak (blue) solvent atoms. The most common acute strong-solvent/solute/strong-solvent angle θ for this first-shell population is about 60°, but the combined first and second shell population also has a significant number of 30° angles, as indicated by the black arrows. On excitation, additional strong solvents are drawn into the innermost shell, displacing weak solvents (as illustrated by the dashed arrows). (b) The net result for the combined first and second shell population is an increase in the number of 60° angles (black arrows) and a decrease in the number of 30° angles.

The significance of these angles can be appreciated a little better, perhaps, by examining what the equivalent probability distribution would look like if the solution were perfectly ordered into a close-packed lattice structure (but with the liquid's density and composition).[77,81] The corresponding (discrete) probability distributions

$$P\left(\cos\theta\right) = \frac{1}{n_{\mathsf{R}}(SS)} \sum_{(j<k)\in \mathsf{R}} \delta_{\cos\theta,\cos\theta(j,k)}$$
$$\cos\theta\left(j,k\right) = \left(\hat{r}_{0j}\cdot\hat{r}_{0k}\right)_{lattice}, \tag{4.5}$$

plotted in Fig. 6 for both *fcc* and *hcp* structures, indicate that the parentage of the angles near 55° in the 1st solvation shell probably lies in the 60° ($\cos\theta \approx 0.50$) close-packed angles. There are 30° angles between pairs of close-packed second shell atoms, but since the liquid-state 2nd shell probability density remains fixed, the assignment of the time-evolving 30° angles in the joint 1st and 2nd shell distribution has to be to solvent angles between an atom in the 1st shell and another in the 2nd – and, indeed, the close-packed structures features such angles.

Given these results, the picture that emerges of the solvent structural change is sketched in Fig. 7. While the most striking long-term change in solvent structure following solute excitation is the replacement of first shell W solvents by first shell S solvents, the whole reason that substitution is slow is because it cannot take place without concomitant addition of W solvent to, and loss of S solvents from, the second (and perhaps further) shells.[22] The particular angular distributions we look at reinforce this point. The evolution of the combined first and second shell structure is more prominent than the evolution of either shell by itself. So, the fact that the field of

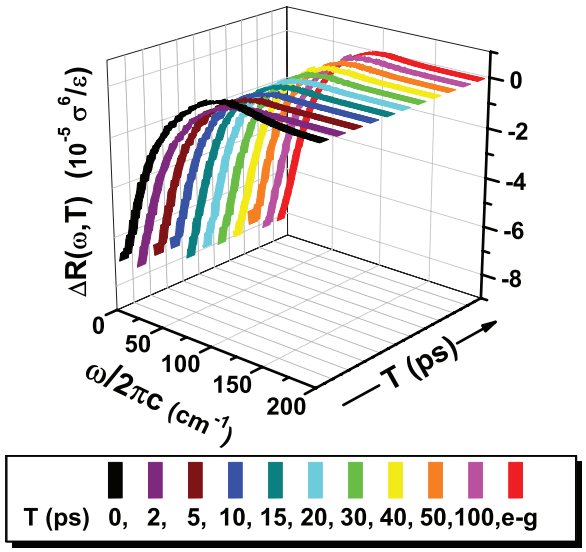

FIG. 8. Two-dimensional solute-pump/solvent-probe spectra for our *polarizability-switched* (10% S) preferential solvation system calculated by hybrid INM/molecular-dynamics methods. The dynamics of this system is identical to the preferential solvation model we use everywhere else in the paper, but the revised model's use of S solvents with polarizabilities much lower than those of the W solvents renders that dynamics largely invisible at long times. All other calculational details are the same as those reported with Fig. 4.

view of solute-pump/solvent-probe spectroscopy is not limited to the first solvation shell may actually be an essential feature of its structure sensitivity.

It is probably worth emphasizing, in this connection, that we would expect optical-Kerr-like spectra to be more sensitive to structural changes in some systems than in others. If, for example, we were to take the same 10% *S* preferential solvation system we have been using, but with the polarizabilities of the *S* and *W* solvents switched (that is, with $\alpha_S = 0.73$ Å^3 and $\alpha_W = 3.99$ Å^3, instead of the reverse), the spectra would look very different – despite the fact that the Hamiltonians, and therefore the dynamics, of the two systems would be absolutely identical. The principal structural change on reaching the equilibrated excited state of the solute (the 130% increase in 1st-shell *S* solvents) would now be spectroscopically dark, leaving only a much smaller fractional change (the 12% decrease in 1st-shell *W* solvents) as the agent responsible for the long-time spectral signature. Perhaps not surprisingly, the resulting spectra, Fig. 8, show almost no discernable time evolution after the first few ps.

V. CONCLUDING REMARKS

The ability to monitor a second solvation coordinate in our spectroscopy, one besides the solute-solvent interaction,[26,82] does not guarantee that we can follow the complete structural evolution of a solvent, but it certainly has the potential to broaden our perspective on what the solvent is doing during solvation. The many-body polarizability seems to be an especially appropriate choice for that second coordinate. In the admittedly specialized model we explored in this paper, the polarizability dynamics directly monitors the liquid structure because changing intermolecular distances makes the polarizability change in the only way that it can – through the interaction-induced contributions.[10,25] But even here, it need not have been the case that the gradual development of the polarizability spectra would track the structural evolution so much more closely than ordinary time-dependent fluorescence. The surprising result of this study is how explicit we can be in assigning this particular component of our two-dimensional signals to structural rearrangement.

Part of what makes this assignment possible is the same feature that it makes it technically feasible to carry out the calculation: there can be a significant separation of time scales between the intermolecular vibration time *t* and the solvation evolution time *T*. Unlike two-dimensional vibrational spectroscopies (for example),[83] we can regard the dynamics on one time axis (*t*) as depending adiabatically on the location on the other time axis (*T*). That allows us to use an unusual hybrid formalism in which the long-time molecular dynamics part of the calculation abdicates its responsibilities for the high-frequency dynamics to instantaneous-normal-mode theory while retaining its ability to incorporate the long-time behavior exactly.

However, what makes this mathematical separation so important to us, and makes this solute-pump/solvent-probe spectroscopy so potentially revealing, is that the *t* and *T* observables themselves are sampling qualitatively different aspects of the liquid dynamics. Unlike two-dimensional examples such as electronic photon echoes,[7–9] which require the solute's optical gap to fill both roles, the combination of polarizability-fluctuation and optical-gap observables seem to lend itself automatically to a division into specifically structural and specifically energetic measurements. The evolution of the solute-solvent interaction is apparently not synonymous with structural evolution of the surrounding solvent, at least for the atomic preferential solvation system we examined here, and our observables seem eminently capable of capturing this distinction.

It is interesting though, and perhaps somewhat surprising, to find our solute-solvent interaction energy relaxing more *slowly* than what we are calling the "structural" dynamics. The scenario we hypothesized in Sec. I for structural dynamics being faster than solvation (potential-energy) dynamics raised the possibility of needing energy-neutral rearrangements within a single solvation shell in preparation for shell-to-shell population transfers. The atomic-liquid angle changes we study in Sec. IV are, in fact, classic examples of structural rearrangements tied only indirectly to the potential energy. Yet, we have no evidence that our model carries out any (picosecond scale) preliminary single-solvation-shell angle changes.[61] Still, our interaction energy is a sensitive function of the precise solute-solvent distances within the crowded first solvation shell, and it could well be more time consuming for the solvent to optimize those dozen "nonstructural" distances than it is for a single solvent to cross the somewhat artificial first-shell/second-shell dividing surface.

The question of how clean this structure/energetics division remains when we move to more molecular solvents and solutes, in any case, is still open. The short-time dynamics of the excited-state/ground-state solute–solvent potential energy difference[64] and the many-body polarizability dynamics[84] are both dominated by first solvation-shell reorientations for dipolar solutes dissolved in polar solvents. So one might not expect much qualitative difference between the two at early times.[85] However, even there, the experimental evidence in a neat acetonitrile solvent[17] is that the *t* and *T* dynamics do show up on dramatically different time scales, with the former consistent with the 75 fs (1/e) dephasing time associated with the roughly 100 cm^{-1} (FWHM) INM bandwidth of acetonitrile's intermolecular vibrations,[64] and the latter relaxing on a ps scale even more protracted than the 600 fs or so characteristic of the slowest component of acetonitrile's time-dependent fluorescence decay.[86]

One might also wonder about our observation that simply reversing the polarizabilities completely masks the two-dimensional response in our model system. Our findings indicate that the solute-pump/solvent-probe spectroscopy we have been discussing clearly has the ability to reveal a side of the liquid-state structural relaxation process that other spectroscopies do not – but it, just as clearly, has its own set of selection rules.

ACKNOWLEDGMENTS

The early stages of this research were greatly aided by Norbert Scherer's sharing his early results on the experiments that motivated these calculations and by collaborative work

with Branka Ladanyi. We also thank Margaret Hershberger for discussions regarding the experimental development and regarding the experimental evidence that at least two coordinates are needed to describe solvation dynamics. This work was supported by NSF Grant No. CHE-1265798.

APPENDIX: COMPARISON OF SOME ANALYTICAL APPROXIMATIONS FOR TWO-DIMENSIONAL CLASSICAL SPECTROSCOPIC RESPONSE FUNCTIONS

In the classical limit, two-dimensional spectroscopic response functions invariably have the form of a classical ensemble average involving observables at three different times (0, t_1, and t_2) inside nested Poisson brackets[24]

$$R\left(0,t_1,t_2\right)=\left\langle\left\{A\left(0\right),\left\{B\left(t_1\right),C\left(t_2\right)\right\}\right\}\right\rangle. \tag{A1}$$

Fifth order Raman spectra, for example, have A, B, and C all equal to many-body polarizabilities. Our solute-pump/solvent-probe response function also fits into this same mold. Because such expressions can always be transformed to averages over a single Poisson bracket simply by integrating by parts[24]

$$R\left(0,t_1,t_2\right)=\beta\langle\dot{A}\left(0\right)\left\{B\left(t_1\right),C\left(t_2\right)\right\}\rangle, \tag{A2}$$

the two-dimensional (last) term in Eq. (2.4) has this form with $\dot{A}=\Delta V$, and B and C equal to many-body polarizabilities.

We can get some insight into INM theories for these response functions[87] by evaluating an Eq. (A1) for a simple, analytically tractable, example, and comparing the results with what the various approximate treatments would give us. Suppose we take our system to be just a one-dimensional harmonic oscillator with frequency ω, and set the $A(t)$, $B(t)$, and $C(t)$ functions all equal to $\delta V\left(t\right)$, the fluctuations in potential energy V, at the respective times

$$\delta V\left(t\right)=\frac{1}{2}m\omega^2x^2\left(t\right)-\frac{1}{2}k_BT. \tag{A3}$$

This example is somewhat harder for theories to handle than it may appear because even the leading contributions to the observables are all nonlinear in the coordinate $x(t)$, but it is nonetheless straightforward to evaluate.

The exact classical result for Eq. (A1) with this model is

$$\begin{aligned}R\left(0,t_1,t_2\right)&=\beta\left\langle\dot{V}\left(0\right)\frac{\partial V\left(t_1\right)}{\partial x_1}\frac{\partial V\left(t_2\right)}{\partial p_1}\right\rangle\\&=\beta\left\langle\dot{V}\left(0\right)\frac{\partial V\left(t_1\right)}{\partial x_1}\frac{\partial V\left(t_2\right)}{\partial x_2}\frac{\partial x_2}{\partial p_1}\right\rangle\\&=\beta\left\langle\left(\omega^2x_0p_0\right)\left(m\omega^2x_1\right)\left(m\omega^2x_2\right)\frac{\partial x_2}{\partial p_1}\right\rangle,\end{aligned}$$

where the subscripts 0, 1, and 2 refer to times 0, t_1, and t_2, respectively. Since x_j, the coordinate-space location of a harmonic oscillator at any time t_j can be expressed in terms of (x_k, p_k), the location in phase space at time t_k,

$$x_j=x_k\cos\omega(t_j-t_k)+\frac{p_k}{m\omega}\sin\omega\left(t_j-t_k\right),$$

we obtain

$$R\left(0,t_1,t_2\right)=\omega^2\left(k_BT\right)\left[\sin\omega\left(t_2-t_1\right)\sin\omega\left(t_2+t_1\right)\right]. \tag{A4}$$

A full INM treatment of this same response function (which would correspond to using the first equality in Eq. (2.9), but not the second) is, not surprisingly, exact. INM dynamics are, after all, harmonic. However, the second step in Eq. (2.9) introduces what one might call a *linear INM* treatment, one in which derivatives of observables with respect to INM coordinates are assumed to be constant on the short INM time scale.[63–66] This approximation yields

$$\begin{aligned}R_{linear\ INM}\left(0,t_1,t_2\right)&\approx\beta\left\langle\dot{V}\left(0\right)\left(\frac{\partial V\left(t_1\right)}{\partial x_1}\right)^2\frac{\partial x_2}{\partial p_1}\right\rangle\\&=\beta\left\langle\left(\omega^2x_0p_0\right)\left(m\omega^2x_1\right)^2\frac{\partial x_2}{\partial p_1}\right\rangle\\R_{linear\ INM}\left(0,t_1,t_2\right)&=\omega^2\left(k_BT\right)\left[\sin\omega\left(t_2-t_1\right)\sin2\omega\left(t_1\right)\right].\end{aligned} \tag{A5}$$

An alternative way to use presumed harmonic behavior to turn classical response functions into ordinary time correlation functions has been proposed by DeVane, Ridley, Space, and Keyes (DRSK).[48–52] Their development retreats to the quantum mechanical analogue of Eq. (A1) (with time-dependent quantum mechanical operators and commutators in the place of classical dynamical variables and Poisson brackets) expressed in terms of real and imaginary parts of quantum time correlation functions, builds in a relationship between those parts valid for harmonic systems, and then identifies the real part of the quantum time correlation function with its classical analogue. In their approximation, when $A(t)$, $B(t)$, and $C(t)$ are all equal to $\delta V(t)$, Eq. (A1) becomes[48,51]

$$\begin{aligned}R_{DRSK}\left(0,T,T+t\right)&=-\tfrac{1}{2}\beta^2\left(\frac{\partial^2}{\partial T^2}-2\frac{\partial^2}{\partial T\,\partial t}\right)\\&\quad\langle\delta V\left(0\right)\ \delta V\left(T\right)\ \delta V\left(T+t\right)\rangle\\&=\beta^2\Big(\langle\delta\dot{V}\left(0\right)\ \delta\dot{V}\left(T\right)\ \delta V(T+t)\rangle\\&\quad+\frac{1}{2}\langle\delta\ddot{V}\left(0\right)\ \delta V\left(T\right)\ \delta V\left(T+t\right)\rangle\Big).\end{aligned} \tag{A6}$$

For the completely harmonic example we have been showcasing, this expression turns into

$$R_{DRSK}\left(0,t_1,t_2\right)=\omega^2\left(k_BT\right)\left[\sin\omega\left(t_2-t_1\right)\sin\omega\left(t_2+t_1\right)\right], \tag{A7}$$

the exact result.

It is possible to show that both linear INM theory and this DRSK theory have a number of sensible properties illustrated by, but not limited to, this example. Both theories are correctly antisymmetric on switching $t=t_2-t_1$ to $-t$, as required by the (B, C) Poisson brackets in Eq. (A1), for example. The necessary change of sign is guaranteed for linear INM theory by

Eq. (2.11) and can be shown to occur for DRSK theory by applying standard correlation function identities to Eq. (A6).[25]

But, as Eqs. (A4), (A5) and (A7) make clear, the DRSK approach is somewhat better than the linear INM treatment in this special completely harmonic example; Eq. (A6) makes no assumptions about the linearity of the observables, whereas Eq. (2.9) does. Moreover, numerical applications to 5th order Raman spectra (which vanishes identically for linear observables governed by harmonic dynamics) seem to suggest that the DSRK ideas may also be better at handling anharmonic aspects of liquid dynamics, at least when both the t_1 and t_2 time scales are short.[52]

However, with the two-dimensional solvation spectroscopy discussed in this paper, the $T = t_1$ time scale is often much larger than the $t = t_2$-t_1 time scale. When this separation occurs, the sin ωt sin $2\omega T$ form of Eq. (A5) correctly displays the way in which the slow dynamics modulates the fast dynamics. Indeed, the reader might note that, in this limit, the linear INM result is actually the same as the exact result, Eq. (A4). More to the point, it is exactly when our 2D spectroscopy is at its most interesting, when the large T dynamics reflects significant structural change, that it is most important to represent the T dynamics most faithfully. Unlike the DRSK theory, the hybrid-MD/linear-INM formalism incorporates that dynamics exactly.[88]

There is, in fact, no compelling reason for an INM approximation to the dynamics (a linearization of the local force in the displacements) to insist on also linearizing the observables. The earliest INM predictions for correlation functions[63–66] used such simultaneous linearizations to turn the tasks of computing single-time-interval correlation functions into purely equilibrium calculations. In much the same way, our doing so here reduced our problem of calculating a two-time-interval, (T, t), Poisson-bracket-containing function to that of simulating a kind of single-time-interval (T) time correlation function. Omitting the linearization in the observable would leave us with a two-time-interval, but nonetheless not all that arduous, time correlation function to calculate, just as in the DRSK theory. Whether this refinement is worth pursuing, though, is a question for future studies.

[1] R. M. Stratt and M. Maroncelli, J. Phys. Chem. **100**, 12981 (1996).
[2] G. R. Fleming and M. Cho, Annu. Rev. Phys. Chem. **47**, 109 (1996).
[3] S. K. Pal, L. Zhao, and A. H. Zewail, Proc. Natl. Acad. Sci. U.S.A. **100**, 8113 (2003).
[4] K. E. Furse and S. A. Corcelli, J. Am. Chem. Soc. **130**, 13103 (2008).
[5] D. M. Willard and N. E. Levinger, J. Phys. Chem. B **104**, 11075 (2000).
[6] J. Faeder and B. M. Ladanyi, J. Phys. Chem. B **109**, 6732 (2005).
[7] M. Cho, J.-Y. Yu, T. Joo, Y. Nagasawa, S. A. Passino, and G. R. Fleming, J. Phys. Chem. **100**, 11944 (1996).
[8] G. R. Fleming, S. A. Passino, and Y. Nagasawa, Phil. Trans. R. Soc. Lond. A **356**, 389 (1998).
[9] Y. Nagasawa, J. Photochem. Photobiol. C **12**, 31 (2011).
[10] X. Sun and R. M. Stratt, Phys. Chem. Chem. Phys. **14**, 6320 (2012).
[11] S. Park, B. N. Flanders, X. Shang, R. A. Westervelt, J. Kim, and N. F. Scherer, J. Chem. Phys. **118**, 3917 (2003).
[12] S. Park, J. Kim, and N. F. Scherer, in *Ultrafast Phenomena XIV*, edited by T. Kobayashi, T. Okada, T. Kobayashi, K. A. Nelson, and S. De Silvestri (Springer, New York, 2005), pp. 557–559.
[13] A. M. Moran, S. Park, and N. F. Scherer, J. Phys. Chem. B **110**, 19771 (2006).
[14] A. M. Moran, R. A. Nome, and N. F. Scherer, J. Chem. Phys. **127**, 184505 (2007).
[15] A. M. Moran, S. Park, and N. F. Scherer, Chem. Phys. **341**, 344 (2007).
[16] S. Park, J. Kim, A. M. Moran, and N. F. Scherer, Phys. Chem. Chem. Phys. **13**, 214 (2011).
[17] S. Park, J. Kim, and N. F. Scherer, Phys. Chem. Chem. Phys. **14**, 8116 (2012).
[18] D. F. Underwood and D. A. Blank, J. Phys. Chem. A **107**, 956 (2003); **107**, 9736 (2003).
[19] S. J. Schmidtke, D. F. Underwood, and D. A. Blank, J. Am. Chem. Soc. **126**, 8620 (2004).
[20] D. F. Underwood and D. A. Blank, J. Phys. Chem. A **109**, 3295 (2005).
[21] S. J. Schmidtke, D. F. Underwood, and D. A. Blank, J. Phys. Chem. A **109**, 7033 (2005).
[22] C. N. Nguyen and R. M. Stratt, J. Chem. Phys. **133**, 124503 (2010).
[23] M. Sakurai and A. Yoshimori, J. Chem. Phys. **122**, 104509 (2005).
[24] A. Ma and R. M. Stratt, J. Chem. Phys. **116**, 4962 (2002).
[25] P. A. Madden, in *Liquids, Freezing, and the Glass Transition*, edited by J. P. Hansen, D. Levesques, and J. Zinn-Justin (North-Holland, Amsterdam, 1991), pp. 547–627.
[26] E. A. Carter and J. T. Hynes, J. Chem. Phys. **94**, 5961 (1991).
[27] G. Tao and R. M. Stratt, J. Chem. Phys. **125**, 114501 (2006).
[28] Here, and throughout the rest of this section, we use the symbol Π as a convenient notation to represent any single off-diagonal element of the 3×3 polarizability tensor $\boldsymbol{\Pi}$.
[29] A. Ma and R. M. Stratt, Phys. Rev. Lett. **85**, 1004 (2000).
[30] C. Dellago and S. Mukamel, J. Chem. Phys. **119**, 9344 (2003).
[31] Y. Nagata and Y. Tanimura, J. Chem. Phys. **124**, 024508 (2006).
[32] S. Mukamel, V. Khidekel, and V. Chernyak, Phys. Rev. E **53**, R1 (1996).
[33] S. V. Malinin and V. Y. Chernyak, Phys. Rev. E **77**, 056201 (2008).
[34] T. l. C. Jansen, J. G. Snijders, and K. Duppen, J. Chem. Phys. **114**, 10910 (2001).
[35] C. J. Milne, Y. Li, T. l. C. Jansen, L. Huang, and R. J. D. Miller, J. Phys. Chem. B **110**, 19867 (2006).
[36] B. J. Ka and E. Geva, J. Chem. Phys. **125**, 214501 (2006).
[37] T. Hasegawa and Y. Tanimura, J. Chem. Phys. **125**, 074512 (2006).
[38] T. Hasegawa and Y. Tanimura, J. Chem. Phys. **128**, 064511 (2008).
[39] Y. Li, L. Huang, R. J. D. Miller, T. Hasegawa, and Y. Tanimura, J. Chem. Phys. **128**, 234507 (2008).
[40] J. Kim and T. Keyes, Phys. Rev. E **65**, 061102 (2002).
[41] T. Keyes and J. Kim, J. Chem. Phys. **122**, 244502 (2005).
[42] R. A. Denny and D. R. Reichman, Phys. Rev. E **63**, 065101(R) (2001).
[43] R. A. Denny and D. R. Reichman, J. Chem. Phys. **116**, 1979 (2002).
[44] R. A. Denny and D. R. Reichman, J. Chem. Phys. **116**, 1987 (2002).
[45] J. Cao, J. Wu, and S. Yang, J. Chem. Phys. **116**, 3739 (2002).
[46] J. Cao, S. Yang, and J. Wu, J. Chem. Phys. **116**, 3760 (2002).
[47] T. l. C. Jansen, and S. Mukamel, J. Chem. Phys. **119**, 7979 (2003).
[48] R. DeVane, C. Ridley, B. Space, and T. Keyes, J. Chem. Phys. **119**, 6073 (2003).
[49] R. DeVane, C. Ridley, B. Space, and T. Keyes, Phys. Rev. E **70**, 050101(R) (2004).
[50] R. DeVane, C. Ridley, B. Space, and T. Keyes, J. Chem. Phys. **123**, 194507 (2005).
[51] R. DeVane, C. Kasprzyk, B. Space, and T. Keyes, J. Phys. Chem. B **110**, 3773 (2006).
[52] R. DeVane, B. Space, T. l. C. Jansen, and T. Keyes, J. Chem. Phys. **125**, 234501 (2006).
[53] R. M. Stratt, Acc. Chem. Res. **28**, 201 (1995).
[54] M. Buchner, B. M. Ladanyi, and R. M. Stratt, J. Chem. Phys. **97**, 8522 (1992).
[55] R. M. Stratt, in *Ultrafast Infrared and Raman Spectroscopy*, edited by M. D. Fayer (Marcel Dekker, New York, 2001).
[56] S. A. Passino, Y. Nagasawa, T. Joo, and G. R. Fleming, J. Phys. Chem. A **101**, 725 (1997).
[57] S. Ryu and R. M. Stratt, J. Phys. Chem. B **108**, 6782 (2004).
[58] A. Ma and R. M. Stratt, J. Chem. Phys. **116**, 4972 (2002).
[59] J. T. Fourkas, in *Ultrafast Infrared and Raman Spectroscopy*, edited by M. D. Fayer (Marcel Dekker, New York, 2001).
[60] As the earliest INM applications pointed out, successful time-domain predictions require that the contributions of any imaginary ($\omega^2 < 0$) modes be removed. This issue is often of little practical concern for frequency-domain calculations because those modes tend to have the wrong geometries to couple well to spectroscopic observables. See Fig. 3 of Ref. 57, for example. The more fundamental difficulty, and the one we consider here, is that the dynamical contributions from *all* the lowest ω^2-value INM modes (including the lowest frequency real modes) are likely to be inaccurate.

Reference 17 did demonstrate that with an acetonitrile solvent there is reasonably good agreement between the calculated INM spectrum appropriate to time-dependent fluorescence (the "solvation spectrum") and the short T limit of the experimental RP-PORS spectrum. However, it should be noted that the correct two-dimensional INM spectrum in this limit is somewhat different from the one-dimensional solvation spectrum.

[61]X. Sun, Ph.D. dissertation, Brown University (2014).

[62]The "reduced spectral density" is the frequency-domain response function resulting from removing the diffusive long-time exponential decay from the full time-domain molecular dynamics response – precisely the same kind of reduced spectrum often reported in experimental OKE measurements. See Refs. 10 and 59 for details. Numerical specifics concerning the relationship between our reduced and unreduced spectra are provided elsewhere (Ref. 61). OKE spectra for both the ground-state (Ref. 61) and excited-state (Fig. 2) solutions used here show little difference between reduced and full spectral densities above 25 cm^{-1}. For lower frequencies, one would expect more substantial differences, and given the inability of the INM methodology used here to describe long-time dynamics, one would expect those methods to be somewhat better at predicting reduced spectra. The observation that the low-ω INM results here are fairly close to the *full* spectral densities may be coincidental; INM calculations of benzene's OKE spectrum, for example, match the reduced portion of the exact molecular-dynamics-derived OKE spectrum much better than they do the full spectrum. (See Ref. 57.)

[63]R. M. Stratt and M. Cho, J. Chem. Phys. **100**, 6700 (1994).

[64]B. M. Ladanyi and R. M. Stratt, J. Phys. Chem. **99**, 2502 (1995).

[65]R. E. Larsen, E. F. David, G. Goodyear, and R. M. Stratt, J. Chem. Phys. **107**, 524 (1997).

[66]B. M. Ladanyi and R. M. Stratt, J. Phys. Chem. A **102**, 1068 (1998).

[67]B. M. Luther, J. R. Kimmel, and N. E. Levinger, J. Chem. Phys. **116**, 3370 (2002).

[68]B. M. Ladanyi and B.-C. Perng, J. Phys. Chem. A **106**, 6922 (2002).

[69]N. Agmon, J. Phys. Chem. A **106**, 7256 (2002).

[70]M. P. Allen and D. J. Tildesley, *Computer Simulation of Liquids* (Clarendon Press, Oxford, 1987), Chap. 3.

[71]F. Cichos, R. Brown, and Ph. A. Bopp, J. Chem. Phys. **114**, 6834 (2001).

[72]L. R. Martins, A. Tamashiro, D. Laria, and M. S. Skaf, J. Chem. Phys. **118**, 5955 (2003).

[73]L. C. Geiger and B. M. Ladanyi, J. Chem. Phys. **89**, 6588 (1988).

[74]R. L. Murry and J. T. Fourkas, J. Chem. Phys. **107**, 9726 (1997).

[75]E. Anderson, Z. Bai, C. Bischof, S. Blackford, J. Demmel, J. Dongarra, J. Du Croz, A. Greenbaum, S. Hammarling, A. McKenney, and D. Sorensen, *LAPACK User's Guide*, 3rd ed. (Society for Industrial and Applied Mathematics, Philadelphia, 1999).

[76]We define the outer boundaries of the first and second solvation shells by the locations of the first and second minima of the ground-state-solute/solvent radial distribution function ($1.556\sigma = 5.298$ Å and $2.548\sigma = 8.676$ Å), respectively. Virtually identical values apply for excited-state solutes.

[77]A. D. J. Haymet, Chem. Phys. Lett. **107**, 77 (1984).

[78]U. Balucani and R. Vallauri, Chem. Phys. Lett. **166**, 77 (1990).

[79]M. Canales and J. A. Padro, Mol. Simul. **8**, 335 (1992).

[80]A. Di Cicco, A. Trapananti, S. Faggioni, and A. Filipponi, Phys. Rev. Lett. **91**, 135505 (2003).

[81]For a close-packed lattice with our density of $\rho\sigma^3 = 0.8$, the distance between closest atoms is $a = 1.209\sigma$, which allows us to mimic the first and second-shell locations in our liquid by setting the boundary distances in our lattice to $1.287a$ and $2.107a$ from any given atom, respectively. For an *fcc* lattice these boundaries place 12 atoms within the first shell and 42 atoms in the second shell. For an *hcp* lattice, the populations are 12 and 44, respectively. Our liquid has 12 and 42 atoms in its first two shells.

[82]R. A. Kuharski, J. S. Bader, D. Chandler, M. Sprik, and M. L. Klein, J. Chem. Phys. **89**, 3248 (1988).

[83]M. Cho, *Two-Dimensional Optical Spectroscopy* (CRC, Boca Raton, 2009), Chap. 12; P. Hamm and M. Zanni, *Concepts and Methods of 2d Infrared Spectroscopy* (Cambridge University, Cambridge, 2011).

[84]M. Paolantoni and B. M. Ladanyi, J. Chem. Phys. **117**, 3856 (2002).

[85]M. Cho, S. J. Rosenthal, N. F. Scherer, L. D. Ziegler, and G. R. Fleming, J. Chem. Phys. **96**, 5033 (1992).

[86]M. L. Horng, J. A. Gardecki, A. Papazyan, and M. Maroncelli, J. Phys. Chem. **99**, 17311 (1995).

[87]The use of INM dynamics for evaluating this specific Poisson bracket was suggested by T. Keyes and J. T. Fourkas, J. Chem. Phys. **112**, 287 (2000).

[88]One might imagine that a mode coupling theory of solvation dynamics might even be better suited for exploiting such time scale separations. To date, however, those theories have focused on the time-varying solute-solvent potential as the sole observable. See, for example, S. A. Egorov, R. A. Denny, and D. R. Reichman, J. Chem. Phys. **116**, 5080 (2002).